The Astrophysical Journal, 738:107 (6pp), 2011 September 1 doi:10.1088/0004-637X/738/1/107

CORONAL MASS EJECTION DYNAMICS REGARDING RADIAL AND EXPANSION SPEEDS

Nivaor R. Rigozo[1], Alisson Dal Lago[2], and D. J. R. Nordeman[2]
[1] Southern Regional Space Research Center–CRS/INPE-MCT 97105-970 Santa Maria, RS, Brazil; nivaor.rigozo@dge.inpe.br
[2] National Institute for Space Research–INPE/MCT, CP 515, 12245-970 São José dos Campos, SP, Brazil; dallago@dge.inpe.br, nordeman@dge.inpe.br
Received 2010 July 21; accepted 2011 June 22; published 2011 August 17

ABSTRACT

A new technique for the detection of coronal mass ejection (CME) speeds using image processing was applied. This technique permits us to determine the CME dynamics: radial and expansion distances, velocities, and accelerations. The CME dynamics is determined by the selection of a radial direction in a given Large Angle and Spectroscopic Coronagraph image, which starts just before the occulter (close to the center) and extends to the extremity of the image. By taking a series of images and extracting the same radial direction, it is possible to have a time history of any moving feature along this direction. This technique allows us to choose the number of directions that is used in the CME detection to determine its dynamics. This paper presents the results for the dynamical features (radial and expansion) of five CME events observed on 1999 February 5, 2001 February 2, 2002 March 1, 2003 December 2, and 2007 December 31.

Key words: Sun: coronal mass ejections (CMEs) – techniques: image processing – techniques: radial velocities

1. INTRODUCTION

Space weather is significantly controlled by coronal mass ejections (CMEs), which can affect the Earth in different ways. CMEs originating from regions close to the central meridian of the Sun and directed toward the Earth are of immediate concern because they are likely to be geoeffective (Michalek et al. 2003; Sharma et al. 2008). These CMEs can affect Earth's magnetospheric environment and technological systems (Webb 2000; Gopalswamy et al. 2001; Bothmer & Zhukov 2006) and can cause the strongest geomagnetic disturbances (Vennerstroem 2001).

The morphology of many CMEs observed consists of a three-part structure: a bright leading edge, a dark cavity, and a bright core or kernel (Illing & Hundhausen 1986). The bright core is often identified as cool, dense prominence material, although it is difficult to prove such association from white-light coronal observations alone. The pre-CME coronal structure is frequently identified as a helmet streamer with a high-density dome, a low-density cavity, and an embedded prominence at the base of the cavity (Low 1994; Hundhausen 1999).

Early measurements of CME speeds suggested that there are two different types of speed profiles, namely, slow CMEs, associated with eruptive prominences, and fast CMEs, originated in solar active regions (Gosling et al. 1976). The fast CMEs propagate at constant speed and the slow CMEs accelerate (MacQueen & Fisher 1983). The CMEs are initiated at a height of 1.3–1.5 solar radii and accelerated until the height of 3.7–4.7 solar radii. In the onset phase of CMEs in the low corona at times they are likely to be accelerated (Zhang et al. 2001).

Several other CME detection methods have proposed the generation of a number of CME catalogs, which do not always agree in terms of measured speeds or of event identification. Many of these proposed methods are done manually, as it is the case of the proposed methods by Sheeley et al. (1999) and Dal Lago et al. (2004). There are automated CME detection methods as presented by Olmedo et al. (2008) named Solar Eruptive Event Detection System (SEEDS). Until now, no automatic CME detection method has the ability to determine the CME lateral expansion speed. The only method available for such measurements is the one presented by Dal Lago et al. (2004) and Schwenn et al. (2005). Recently, these authors have proposed the use of the halo CME lateral expansion speed, measured in Large Angle and Spectroscopic Coronagraph (LASCO) C3 Images instead of a single direction projection speed to predict the CME travel time to Earth, obtaining very good results.

In this paper, we present our own software package that automatically detects CMEs and their lateral expansion speed, called the Coronal Mass Ejection Dynamic Characteristic Detection System (CMEDCDS). The CMEDCDS is used to make comparisons between CME radial speeds and expansion speed for five CME events.

2. METHODOLOGY

2.1. LASCO C3 Images

Operating since 1996, the very successful LASCO experiment on board the *Solar and Heliospheric Observatory* (*SOHO*) satellite (Brueckner et al. 1995) has provided a comprehensive coverage of observations of the solar corona. *SOHO* is a joint project from the National Aeronautics and Space Administration (NASA) and the European Space Agency (ESA). LASCO provides solar corona dynamic observations from its two coronagraphs, named C2 and C3, which image the corona from 2 to 6 and 4 to 32 solar radii, respectively (St. Cyr et al. 2000).

In this work, we analyzed five CME events observed on 1999 February 5, 2001 February 2, 2002 March 1, 2003 December 2, and 2007 December 31. Table 1 shows the image information about each CME events observed.

2.2. The Technique

Our technique is divided into four steps: (1) preprocessing, which optimizes the input image data for detection, (2) the initial detection, which searches for the brightness enhancement, (3) tracking of the CME in the subsequent running-difference images, and (4) determination of the CME dynamic radial and lateral expansion characteristics.

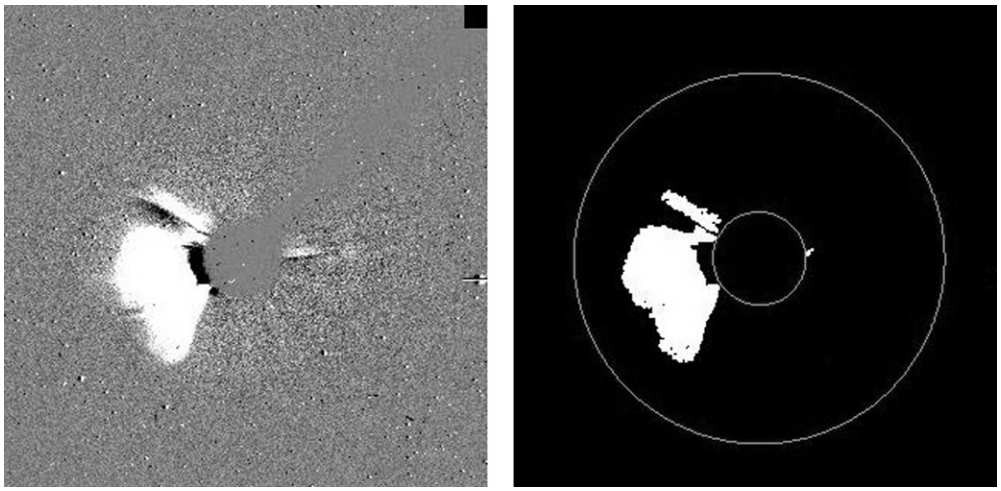

Figure 1. Results of the processing method. The left panel shows the original data from 2007 December at 01:31 UT, as a running-difference image, whereas the right panel shows the masked CME post-processing. Our chosen field of view is represented by the green circles in the top panel.

Table 1
Beginning and End Time of Observation and Number of Images for Every CME Event Observed

CME Events	Time First Image	Time Last Image	Number of Images
1999 Feb 5–6–	23:19:17	02:45:12	6
2001 Feb 2	19:05:43	23:42:05	6
2002 Mar 1	03:18:05	06:42:06	7
2003 Dec 2	11:18:05	13:42:06	4
2007 Dec 31	02:18:04	04:18:04	5

2.3. Preprocessing

The input to the detection system is LASCO C3 "LEVEL 0.5" images—essentially the raw data with 1024 × 1024 or 1024 × 512 pixels. To make image processing efficient, the input images, which are in [x, y] Cartesian coordinates, are transformed into a [θ, r] polar coordinate system because the features of interest are intrinsically in polar coordinates owing to the spherical structure of the Sun. This kind of transformation has been used in other CME-detection algorithms (Robbrecht & Berghmans 2004; Qu et al. 2006; Olmedo et al. 2008). It is then passed through a noise filter to suppress sharp noise features such as stars and cosmic rays. Then, a mask is made to indicate areas of missing blocks in the telemetry. This mask is useful because the missing data blocks may cause anomalous false signals in the difference images and thus lead to a false detection. For the same reason, the planets seen in the images are also masked to avoid any false signals in CME detection. Finally, the image is transformed into a polar coordinate system.

An important step in the preprocessing procedure is the application of a noise filter to the input images. There are two general purposes for this filter: (1) to remove features such as cosmic rays and random noise, and (2) to remove background stars and correct for planets and comets. A three-step process is followed, where the end product is a mask that identifies the feature. First, it involves a new mask that contains the location of the larger features (planets, comets, etc.) and the invalid pixels, which are then replaced with zeros. To more fully cover the larger features, some morphological dilation is applied to this mask. Morphological erode is an image processing technique where a binary image is used to remove pixels on object boundaries on a smaller structuring element (Boomgard & Balen 1992; Adams 1993; Soille et al. 1996). Second, we have the application of a smooth filter (a median filter) to the original input image. This filter essentially smoothes out the small features (cosmic rays and background stars) and leaves only the larger ones. Third, correction of the invalid pixels is made, since they are representative of the background.

2.4. Detection

The operator can define the region where the digital processing is done in order to reduce the processing time. Regions inside the coronagraph occulter or close to the outer edges of the images can be removed. The concerned region is a ring between two concentric circles, the smaller one being the occulter and the greater one being adjusted to cover the CME event (Figure 1). The definition of this region allows a much faster digital image processing of only the region of interest.

The initial CME detection is made on the polar-transformed running-difference sequence images. First, the two-dimensional (2D) images are projected to one dimension along the angular axis such that the values of the radial pixels in each degree column in the image are summed. This effectively measures the total brightness of signals along one particular angular degree. This type of image essentially removes static or quasi-static background features such as coronal streamers and enhances features that change at faster timescales. A CME in a running-difference image appears as a bright leading-edge enhancement (positive pixel values) followed by a dark area deficient in brightness (negative pixel values); then, the background appears gray, indicating zero-change pixels. Since the detection concerns the bright leading edge, only the positive pixels are counted when making the 1D projection. Hence, the 2D enhancement is seen as a peak in the 1D intensity profile. Also, by excluding the negative enhancement, the positive enhancement becomes more outstanding in the projection profile. An example of the projection intensity profile to 180° position angle (P.A.) can be seen in Figure 2. The final frontier is chosen between the positive intensity and zero, since it represents the edge of the CME. Figure 2 shows the final frontier between 300 and 310 pixels.

An important issue that arises at this point is the emergence of multiple CMEs at the same time, which in our detection algorithm is not seen as a problem. It can identify all the CMEs, provided that the CMEs occur in different radial directions. This

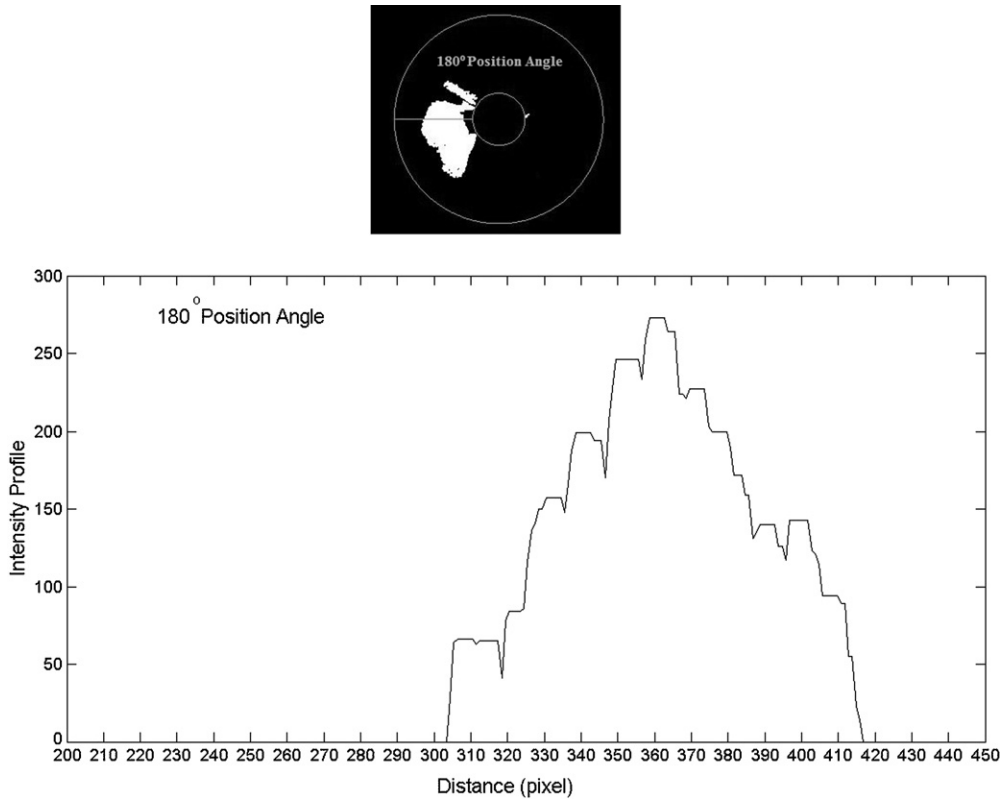

Figure 2. Example of the projection intensity profile to 180° position angle (top). Our chosen field of view is represented by the gray circles in the top panel. The bottom panel shows the 2D images intensity profile, along the 180° angular axis, as a function of distance (in pixel values). CME in a running-difference image appears as a bright leading-edge enhancement (positive pixel values).

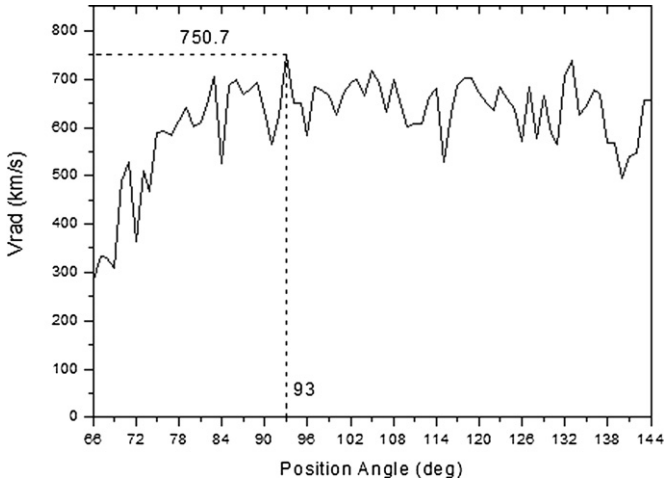

Figure 3. Speed radial of CME in function of angle. It permits us to visualize the fastest CME plane-of-sky speed direction. The dashed line shows the fastest speed of 750.7 km s^{-1} in the P.A. of 93°.

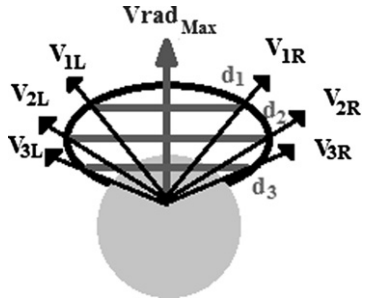

Figure 4. Speed lateral expansion and its determination by CMEDCDS. The gray arrow represents the position angle (P.A.) of the fastest CME plane-of-sky speed. Starting from this position angle, it detects the edges of the CME in pairs of two equidistant P.A. (black arrows), centered at the fastest CME speed central P.A.

is because the detection is made radially across the solar disk, i.e., in all 360°.

2.5. CME Expansion Dynamics

As mentioned above, the software package determines the edged contours of the CME in all directions, for all images. It is possible thus to automatically measure the plane-of-sky speed of the edges of the CME in all P.A.s and search for the fastest CME plane-of-sky speed direction, as shown in Figure 3.

In order to determine the CME expansion dynamics, we (1) determined the P.A. of the fastest CME plane-of-sky speed; and (2) starting from this P.A., detected the edges of the CME in pairs of two equidistant P.A., centered at the fastest CME speed central P.A. After finding which pair of equidistant angular edges has the largest distance between them, this value is indicative of the expansion size (Figure 4). Time evolution of this expansion size, which is detected for each of the LASCO images, represents the CME expansion speed. Note that some parts of CME edge may be too faint to be detected by the software. In this case, even if its equidistant angular pair edge is detected, these values are not considered. This procedure is a little different from the definition of CME expansion speed by Schwenn et al. (2005) and Dal Lago et al. (2003) (Figure 5), who stated that the expansion should be perpendicular to the fastest speed direction. In the case of asymmetric CMEs, the expansion size may be off the perpendicular direction. An example of the procedure is shown

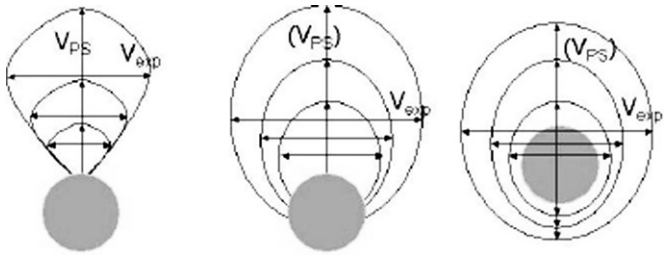

Figure 5. Expansion speed V_{exp} definition. It can be determined uniquely for all types of CMEs, limb, partial halo, or full halo CMEs, while the apparent plane-of-sky speed V_{PS} (in this article V_{PS} is referenced only as V) often contains an unknown speed component toward the observer (Schwenn et al. 2005).

in Figure 6. In the same way, expansion acceleration can be easily measured.

In the case of multiple CMEs, the algorithm is not able to distinguish among them. A solution for this limitation is to manually separate the CMEs and run the software for each of them separately.

2.6. Example Case

The event that occurred on 2007 December 31 at 01:31 UT is an example case (Figure 6). We show the CME evolution in five different images with the leading edge overplotted with a black dotted line. Table 2 shows the result determined by our system and the results of the SEEDS (Olmedo et al. 2008), and CDAW and catalog.

Observing Table 2, three points stand out: (1) the P.A. has only a difference of degree, a very small value; (2) the three methods present different values both in velocity and acceleration; and (3) only our system, CMEDCDS, can determine the speed of lateral expansion of the acceleration of the CME.

3. RESULTS

The study of the evolution of CME was made for 360 directions, representing an angular distance of 1° between two adjacent directions. The angular distance between two directions (or aperture angle) is adjustable to any desired resolution. Thus, applying our technique on the images of these CME events we obtain height–time scatter plots, as shown in Figure 6, where the horizontal axis is the time (in hours) and the vertical axis is the radial distance from the Sun center (in solar radii). These height–time scatter plots represent the highest speed found. In the CME event, on 1999 February 5 the highest speed of 662.9 km s^{-1} for the direction of 161° was observed; on 2001 February 2 the highest speed of 738.4 km s^{-1} for the direction of 49° was observed; on 2002 March 1 the highest speed of 759.4 km s^{-1} for the direction of 241° was observed; on 2003 December 2 the highest speed of 1265.2 km s^{-1} for the direction of 266° was observed; and on 2007 December 31 the highest speed of 750.7 km s^{-1} for the direction of 93° was observed. For comparison, we used the following catalog results: (1) the *SOHO* LASCO CME catalog (http://cdaw.gsfc.nasa.gov/CME_list/), which presents the radial velocities of 660 km s^{-1}, 639 km s^{-1}, 719 km s^{-1}, 1393 km s^{-1}, and 995 km s^{-1}, respectively, for the days mentioned above; and (2) the automated CME detection methods as presented by Olmedo et al. (2008)—SEEDS, which presents the radial velocities of 663 km s^{-1}, 368 km s^{-1}, 113 km s^{-1}, 178 km s^{-1}, and 481 km s^{-1}, respectively, for the days mentioned above. Our results are in very good accordance with the *SOHO* CME catalog, with a correlation coefficient of 0.92.

Table 2
Dynamic Characteristics of 2007 December 31, 01:30 UT CME Event: Results Obtained by SEEDS, CDAW, and CMEDCDS Methods

Methods	P.A.	v_{rad}	a_{rad}	V_{exp}	A_{exp}
CMEDCDS (our)	93	750.7	−9.5	67.4	−0.1
CDAW (*SOHO* catalog)	92	995	−17.9	...	...
SEEDS (Olmedo et al. 2008)	92	481	−56.9	...	...

The acceleration and deceleration values were also calculated for each CME event. The acceleration was obtained in two CME events: in 1999 February 5, it was 87.4 m s^{-2} and in 2003 December 2, it was 20.3 m s^{-2}. The *SOHO* LASCO CME catalog also presents accelerations for these CME events, which were 20.2 m s^{-2}, and 18.5 m s^{-2}, respectively. The SEEDS presents acceleration only in CME event of 2003 December 2, as 8.0 m s^{-2}. The deceleration was obtained in three CME events: on 2001 February 2, −6.3 m s^{-2}; on 2002 March 1, −28.9 m s^{-2}; and on 2007 December 31, −9.5 m s^{-2}. The *SOHO* LASCO CME catalog also presents deceleration for these CME events, with values −6.2 m s^{-2}, −16.2 m s^{-2}, and −17.9 m s^{-2}, respectively. The SEEDS presents deceleration in two CME events: in 2001 February 2, −21 m s^{-2} and 2007 December 31, −56.9 m s^{-2}. Dal Lago et al. (2004) point that the acceleration and deceleration are closely related to the CME initiation mechanism and to the interaction with the surrounding ambient.

Dal Lago et al. (2003) and Schwenn et al. (2005) have defined the CME expansion speed (V_{exp}) as the growth rate approximately perpendicular to the radial speed direction (Figure 7). Also, according to these authors, the expansion speed would be the most relevant parameter from CME dynamics to study the occurrences of geomagnetic storms. Thus, applying our definition of expansion speed explained above in our data set, we obtained CME expansion speed (V_{exp}) for the events: 1999 February 5, 114.4 km s^{-1}; 2001 February 2, 611.7 km s^{-1}; 2002

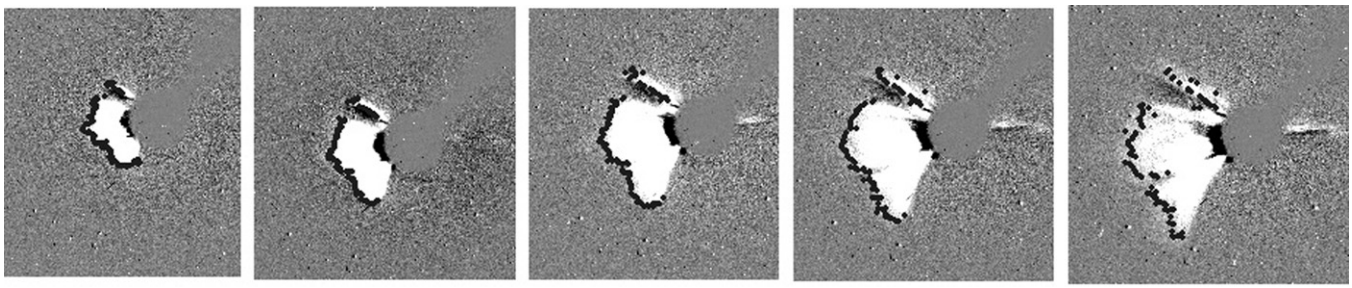

Figure 6. Automatic tracking of the event on 2007 December 31 at 01:31 UT. The black dotted lines indicate the detected leading edges of the CME overlaid on the running-difference images.

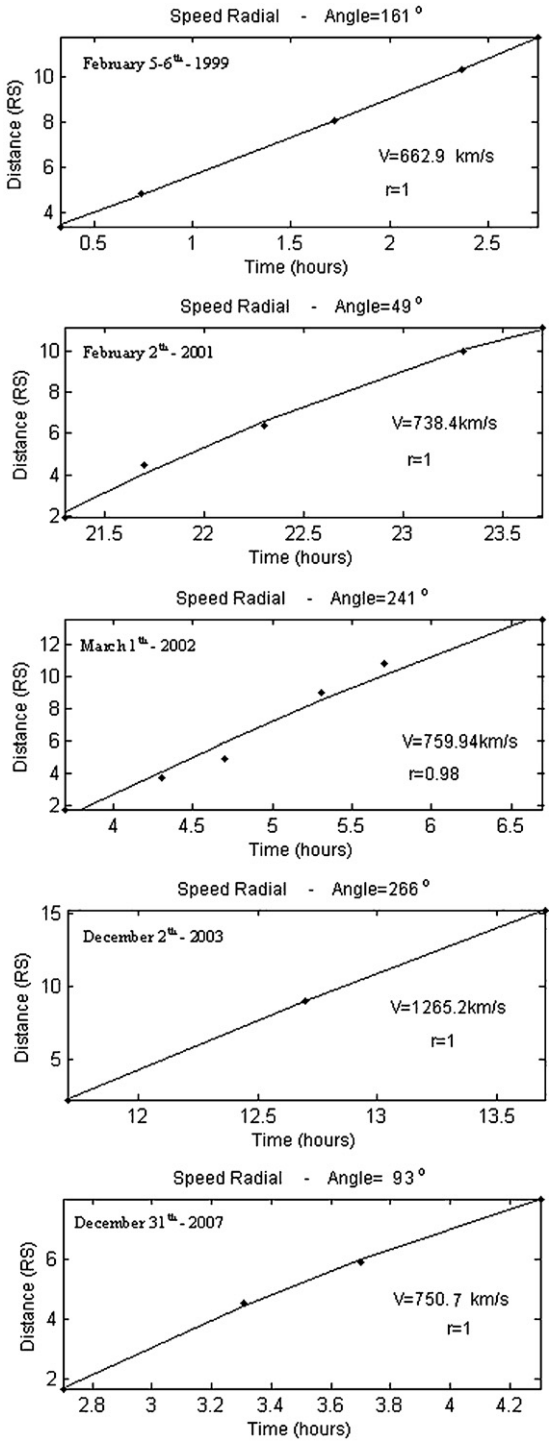

Figure 7. Height–time scatter plots representing the radial fastest speed of the five CME events determined by CMEDCDS. The presentation of events on 1999 February 5, 2001 February 2, 2002 March 1, 2003 December 2, and 2007 December 31 is made from the bottom up.

March 1, 538.8 km s^{-1}; 2003 December 2, 1091.3 km s^{-1}; and 2007 December 31, 67.4 km s^{-1}.

Figure 8 presents a scatter plot of the CME radial speed as a function of the corresponding CME expansion speed. The correlation coefficient for all data set is $R = 0.84$ and the linear fitting function shown in the figure as the solid line is given by

$$V_{\rm rad} = 0.50 * V_{\rm exp},$$

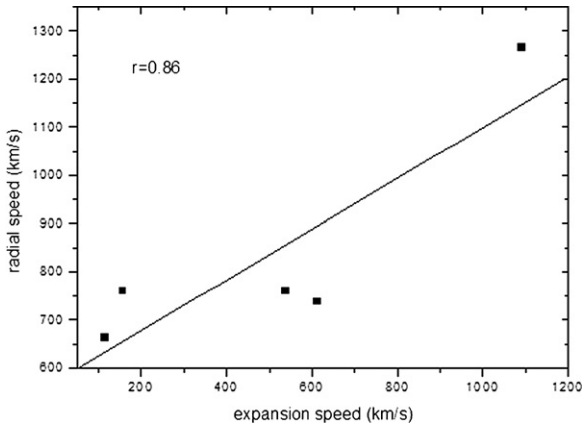

Figure 8. Correlation between radial CME speed (V) and the expansion speed ($V_{\rm exp}$) for five CME events observed by LASCO.

where "$V_{\rm rad}$" is the CME radial speed and "$V_{\rm exp}$" is the CME expansion speed. Dal Lago et al. (2003) and Schwenn et al. (2005) have studied the relationship between radial speed and expansion speed to 57 limb CME. They have obtained a correlation of 0.85 between the radial speed and expansion speed, but an angular coefficient of 0.88, which is considerably distinct from the one obtained in this work. Our study was applied for only five CME events, and, unlike Dal Lago et al. (2003) study, they were not necessarily correlated with close-to-the-limb disk activity. This is probably the reason for the discrepancy in the angular coefficients. The closer the CME is from the limb, the faster the $V_{\rm rad}$ projection in the plane of sky is expected. Thus, the angular coefficient for limb CMEs should be higher than for non-limb CMEs.

4. CONCLUSION

Height–time diagrams for five CME events observed by LASCO C3 on 1999 February 5, 2001 February 2, 2002 March 1, 2003 December 2, and 2007 December 31 were obtained from a new technique which permits easy visualization of radial outward movements in the solar corona.

From the analysis of these five events, the acceleration was observed only for the CME events on 1999 February 5, 87.4 m s^{-2}, and 2003 December 2, 20.3 m s^{-2}. The deceleration was observed only for the CME events: on 2001 February 2, −6.3 m s^{-2}; on 2002 March 1, −28.9 m s^{-2}; and on 2007 December 31, −9.5 m s^{-2}. These results are in accordance with *SOHO* LASCO CME catalog with a correlation coefficient of 0.92 between radial speeds and 0.88 between radial accelerations.

We also presented a relationship between CME radial speeds and expansion speeds based on observations made by the LASCO C3 coronagraph from five CME events on 1999 February 5, 2001 February 2, 2002 March 1, 2003 December 2, and 2007 December 31. A high correlation of 0.84 between these two speeds has been found, being the radial speed 50% of the lateral expansion speed. These results are distinct from the ones obtained by Dal Lago et al. (2003) and Schwenn et al. (2005), probably because the former used a random set of CMEs, while the latter used a set of CMEs correlated with close-to-the-limb solar disk activity.

The authors acknowledge LASCO and EIT teamwork for the solar data used in this work. The authors also acknowledge CNPq of Brazil for supporting this work, under the projects

APQ 470252/2009-0 and research productivity, 301033/2009-9. A. Dal Lago acknowledges CNPq of Brazil for support under projects 303798/2008-4 and 481368/2010-8.

REFERENCES

Adams, R. 1993, Comput. Vis. Graph. Image Process.: Graph. Models Image Process., 55, 325
Boomgard, V. D., & Balen, R. V. 1992, Comput. Vis. Graph. Image Process.: Graph. Models Image Process., 54, 252
Bothmer, V., & Zhukov, A. 2006, The Sun as the prime source of space weather, in Space Weather-Physics and Effects, ed. V. Bothmer & Y. Daglis (Berlin: Springer), 31
Brueckner, G. E., Howard, R. A., Koomen, M. J., et al. 1995, Sol. Phys., 162, 357
Dal Lago, A., Schwenn, R., & Gonzalez, W. D. 2003, Adv. Space Res., 32, 2637
Dal Lago, A., Schwenn, R., Stenborg, G., et al. 2004, Geofís. Int., 439, 41
Gopalswamy, N., Lara, A., Yashiro, S., Kaiser, M. L., & Howard, R. A. 2001, J. Geophys. Res., 106, 29207
Gosling, J. T., Hildner, E., MacQueen, R. M., et al. 1976, Sol. Phys., 48, 389
Hundhausen, A. J. 1999, in Coronal Mass Ejections, ed. K. T. Strong, J. L. R. Saba, & B. M. Haisch (New York: Springer), 143
Illing, R. M. E., & Hundhausen, A. J. 1986, J. Geophys. Res., 91, 10951
Low, B. C. 1994, Phys. Plasmas, 1, 1684
MacQueen, R. M., & Fisher, R. R. 1983, Sol. Phys., 89, 89
Michalek, G., Gopalswamy, N., & Yashiro, S. 2003, ApJ, 584, 472
Olmedo, O., Zhang, J., Wechsler, H., Poland, A., & Borne, K. 2008, Sol. Phys., 248, 485
Qu, M., Shih, F. Y., Jing, J., & Wang, H. 2006, Sol. Phys., 237, 419
Robbrecht, E., & Berghmans, D. 2004, A&A, 425, 1097
Schwenn, R., Dal Lago, A., Huttunen, E., & Gonzalez, W. D. 2005, Ann. Geophys., 23, 1033
Sharma, J., Mittal, N., Tomar, V., & Narain, U. 2008, Ap&SS, 317, 261
Sheeley, N. R., Jr., Walters, J. H., Wang, Y.-M., & Howard, R. A. 1999, J. Geophys. Res., 104, 24739
Soille, J., Soille, R., & Soille, P. 1996, Pattern Recognit. Lett., 17, 1057
St. Cyr, O. C., Howard, R. A., Sheeley, N. R., et al. 2000, J. Geophys. Res., 105, 18169
Vennerstroem, S. 2001, J. Geophys. Res., 106, 29175
Webb, D. F. 2000, IEEE Trans. Plasma Sci., 28, 1795
Zhang, J., Dere, K. P., Howard, R. A., Kundu, M. R., & White, S. M. 2001, ApJ, 559, 452